Synthesis and characterisation of a Ni_4 single-molecule magnet with S_4 symmetry†

Alan Ferguson,[a] Jon Lawrence,[b] Andrew Parkin,[a] Javier Sanchez-Benitez,[c] Konstantin V. Kamenev,[c] Euan K. Brechin,[d] Wolfgang Wernsdorfer,[e] Stephen Hill[b] and Mark Murrie*[a]

Received 2nd May 2008, Accepted 15th August 2008
First published as an Advance Article on the web 8th October 2008
DOI: 10.1039/b807447j

$[Ni_4Cl_4(HL)_4]$ (**1**) $\{H_2L{=}HN(CH_2CH_2OH)_2\}$ has S_4 symmetry and crystallises in the tetragonal space group $I4_1/a$. Two exchange couplings are observed between the four Ni(II) centres, with $J1 = 7.29$ cm^{-1} and $J2 = -2.08$ cm^{-1}, leading to an $S = 4$ ground state. The Ni_4 complex shows the onset of frequency dependent signals in the out-of-phase ac susceptibility below 3 K. In single-crystal measurements carried out using a micro-SQUID, hysteresis loops are observed below 0.5 K, confirming that **1** shows slow relaxation of magnetisation. The loops are temperature dependent but only weakly sweep rate dependent due to the presence of small intermolecular interactions, which hinder quantum tunnelling. This exchange bias between Ni_4 molecules is also seen in high-frequency high-field EPR measurements, which give the parameters $D = -0.75$ cm^{-1}, $B_4^\circ = -6.7 \times 10^{-5}$ cm^{-1} and $g_z = 2.275$.

Introduction

Since the discovery of the first single-molecule magnet (SMM), $[Mn_{12}O_{12}(CH_3COO)_{16}(H_2O)_4]{\cdot}2CH_3COOH{\cdot}4H_2O$ ($Mn_{12}OAc$),[1] in 1993 there has been a huge amount of interest in the synthesis and characterisation of clusters containing paramagnetic metal ions. These polynuclear clusters have been shown to display slow magnetic relaxation below a certain blocking temperature. There are now many examples of SMMs using Mn ions,[2] as the presence of Mn(III) and Mn(IV) ions often leads to clusters with a high spin ground state combined with a large and negative Ising-type anisotropy required for SMM behaviour.[3] In addition to these examples, SMMs have also been synthesised using Fe,[4] Ni,[5] Co,[6] and V ions.[7]

Recent research has focussed on raising the blocking temperature of these clusters with a new Mn_6 complex being reported by Milios *et al.*[8] to have an effective barrier to the reorientatation of the magnetisation of 86.4 K and a blocking temperature of ~4.5 K. This recent breakthrough of improved working temperatures of SMMs and their application to molecular spintronics[9] demonstrate the great interest in this area of research. We are interested in the coordination chemistry of amino-polyalcohols and have developed new synthetic routes to mixed-valence cobalt and iron(III) complexes using the polydentate proligands 2-[bis(2-hydroxyethyl)amino]-2-(hydroxymethyl) propane-1,3-diol (Scheme 1, Bis-tris, H_5L^1) and 2-amino-2-(hydroxymethyl) propane-1,3-diol (Scheme 1, Tris, H_3L^2).[10] We now extend this study to nickel(II) by using 2,2′-iminodiethanol (Scheme 1, commonly referred to as diethanolamine or DEA, H_2L). Although the chemistry of DEA derivatives has been thoroughly investigated with iron,[11] there are only a handful of complexes with nickel.[12] These include a Ni_{24} complex containing methyl-substituted diethanolamine.[13]

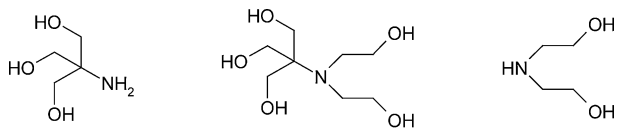

Tris Bis-Tris DEA

Scheme 1

The potential of the nickel(II) ion was highlighted when the first Ni(II) SMM, an Ni_{12} complex, was reported in 2001 by Cadiou *et al.*[5a] Since then only a few more SMMs containing Ni(II) have been reported. These include Ni_{10},[14] Ni_8,[15] and Ni_{21} complexes,[5c] with a mixed metal Mn_2Ni_2 complex also being reported to show SMM behaviour.[16] Cubanes are established as SMMs with manganese, iron, cobalt and nickel centres. $[Ni_4Cl_4(HL)_4]$ (**1**) joins the class of nickel(II)-based cubane complexes which possess $S = 4$ ground states and a large Ising-type magnetic anisotropy.[17] However, the low temperature hysteresis loops and high-field, high-frequency EPR spectra are consistent with intermolecular interactions between the Ni_4 SMMs. Such exchange bias has been seen previously for an Mn_4 SMM.[18]

Experimental

Materials and instrumentation

All chemicals and solvents used for synthesis were purchased from Sigma-Aldrich and were used without further purification.

[a]*WestCHEM, Department of Chemistry, University of Glasgow, University Avenue, Glasgow, UK, G12 8QQ. E-mail: M.Murrie@chem.gla.ac.uk; Fax: +44 141 330 4888; Tel: +44 141 330 4486*
[b]*Department of Physics, University of Florida, Gainsville, FL 32611*
[c]*School of Engineering and Electronics and Centre for Science at Extreme Conditions, University of Edinburgh, West Mains Road, Edinburgh, UK EH9 3JJ*
[d]*School of Chemistry, University of Edinburgh, West Mains Road, Edinburgh, UK EH9 3JJ*
[e]*Institut Néel, CNRS & University J. Fourier, BP 166, 38042, Grenoble Cedex 9, France*

† CCDC reference number 686886. For crystallographic data in CIF or other electronic format see DOI: 10.1039/b807447j

The infrared spectra were measured on a powdered sample using a JASCO 4100 FTIR spectrometer with a PIKE Miracle ATR attachment. Elemental analysis for C, H and N were carried out in the Chemistry Department at the University of Glasgow.

Synthesis

The title compound was obtained using two methods, however, all characterisation was carried out on crystalline or powdered samples from Method A as no crystals were obtained from Method B.

$[Ni_4Cl_4(HL)_4]$ Method A. To a stirred solution of $NiCl_2{\cdot}6H_2O$ (1.902 g, 8 mmol) in MeOH (20 ml) was added Tris (0.485 g, 4 mmol), DEA (0.421 g, 4 mmol) and finally NaOMe (0.432 g, 8 mmol). The solution was stirred overnight to give a green solution that was filtered to remove a tiny amount of green precipitate. Portions of the solution were taken and layered with MeCN in sealed sample tubes. After a few days, large light-green crystals of $[Ni_4Cl_4(HL)_4]{\cdot}4MeCN{\cdot}4.5H_2O$ formed in 21% yield. The crystals lose solvent rapidly when removed from the mother liquor. Selected IR data: ν = 3197, 2889, 1454, 1329, 1116, 1083, 1044, 989, 781 cm^{-1}. Analysis, calc. (found) for $C_{16}H_{46}Cl_4N_4Ni_4O_{11}$ (**1**·$3H_2O$): C, 22.69 (22.52), H, 5.47 (5.02), N, 6.61 (6.49).

Method B

To a stirred solution of $NiCl_2{\cdot}6H_2O$ (1.902 g, 8 mmol) in MeOH (20 ml) was added DEA (0.842 g, 8 mmol) and NaOMe (0.432 g, 8 mmol). The solution was stirred overnight to give a light green solution and green precipitate. The green precipitate has an identical IR spectrum to the crystals produced by method A. Analysis, calc. (found) for $C_{16}H_{48}Cl_4N_4Ni_4O_{12}$ (**1**·$4H_2O$): C, 22.21 (22.41), H, 5.59 (5.26), N, 6.48 (6.35).

X-Ray crystallography†

Intensity data were collected at 100K using a Bruker APEX2 CCD diffractometer equipped with graphite-monochromated Mo Kα radiation (λ = 0.71073Å) and an Oxford Cryosystems low temperature device. The structure was solved by direct methods using SIR92[19] and refined using full matrix least squares refinement on F^2 using CRYSTALS.[20] Non-hydrogen atoms were refined anisotropically; H atoms were all located in a difference map, but those attached to carbon atoms were repositioned geometrically. The H atoms were initially refined with soft restraints on the bond lengths and angles to regularise their geometry, after which the positions were refined with riding constraints. 182 electrons per unit cell were modelled as approximately 18 molecules of disordered water solvent per unit cell using the BYPASS method of van der Sluis and Spek[21] implemented within PLATON.[22]

Magnetic measurements and EPR spectroscopy

Magnetic susceptibility and magnetisation measurements were carried out on a Quantum Design MPMS SQUID magnetometer. Measurements were performed on a polycrystalline sample, which was ground to a powder and restrained in eicosane. The mass of sample used was 13.36 mg and the measurements were carried out in the temperature range 1.8–300 K with fields up to 5 T. A diamagnetic correction of -423.6×10^{-6} cm^3 mol^{-1} was applied to the magnetic susceptibility data. AC measurements were carried out using a Quantum Design Physical Property Measurement System (PPMS) magnetometer, with the same sample restrained in eicosane, for the temperature range 1.8–8K (zero dc field, 3 G ac drive field and ν = 130, 225, 476, 976, 1267, 1997, 2997, 3997, ···, 9997 Hz). The field and temperature dependences of magnetisation were measured up to 1.4 T between 7 and 0.04 K on single-crystals using a micro-SQUID.[23]

Multi-high-frequency (50–300 GHz) EPR experiments were performed using a cavity perturbation technique, with a broadband millimeter-wave vector network analyzer employed as a source/detector system. Experiments were conducted in a high-field (up to 17 T) superconducting magnet equipped with a variable helium flow cryostat. The EPR cavity enabled in-situ rotation of the sample about a single-axis; this instrumentation is described elsewhere.[24] In order to avoid loss of the highly volatile solvent from the crystals, the sample was rapidly transferred from the mother solution to the EPR cavity, where it was coated in paratone oil, then quench cooled to liquid nitrogen temperature (77 K) in the space of just a few minutes.

Results and discussion

Description of structure

The structure of **1** is shown in Fig. 1 and consists of a distorted $\{Ni_4O_4\}$ cubane, with the μ_3-O donors derived from the four alkoxide groups of the mono-deprotonated DEA ligands. Each amine group and the remaining four O atoms are monodentate, with the final site at each nickel(II) centre filled by a terminal Cl ligand. The monodentate alkoxide groups of the ligand are protonated and hydrogen bond to a Cl ligand within the same complex (O1–H10···Cl1a = 3.03 Å). The coordination environment at each nickel is distorted octahedral due to the imposed ligand bite angles. **1** crystallises in the tetragonal space group $I4_1/a$ (see Table 1) and has crystallographic S_4 symmetry, with the S_4 axis coincident with the *c*-axis. The six faces of the cubane are not all equivalent, with the four side faces (parallel to *c*) having Ni–O–Ni bridging angles of 96.3° and 98.3°, whereas the top and bottom faces (perpendicular to *c*) have Ni–O–Ni angles

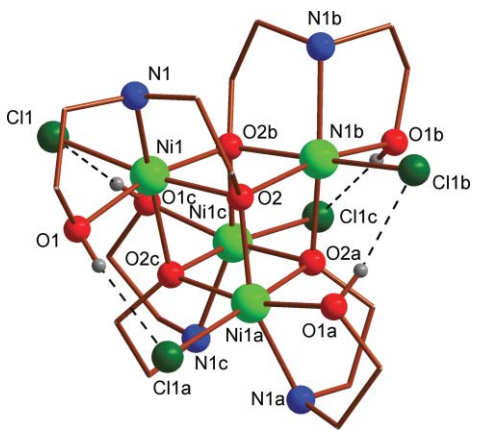

Fig. 1 Structure of **1** showing the distorted cubane core and hydrogen bonding (dashed lines) within the complex (Ni, pale green; N, blue; O, red; C, brown; Cl, dark green; H, grey). H atoms only shown for monodentate alkoxide arms of the DEA ligand.

Table 1 Crystallographic data for **1**

Empirical formula	$C_{24}H_{61}Cl_4N_8Ni_4O_{12.5}$
FW/g mol^{-1}	1030.45
Crystal system	Tetragonal
Space group	$I4_1/a$
a/Å	12.2907(3)
c/Å	28.7030(14)
V/Å^3	4335.9(3)
Z	4
Crystal size/mm	0.2 × 0.2 × 0.25
T/K	100(2)
λ/Å	0.71073
ρ_{calcd}/Mg m^{-3}	1.574
μ/mm^{-1}	2.016
R_1,[a] wR_2	0.0434, 0.1331
Goodness of fit indicator	1.00
Parameters/restraints	94/2
N_{obs}, N_{unique}, R_{int}	30419, 3332, 0.028

[a] $R_1 = \sum\|F_o\| - \|F_c\|/\sum\|F_o\|$ $wR_2 = [\sum[w(F_o^2 - F_c^2)^2]/\sum[w(F_o^2)^2]]^{1/2}$ where $w = 1/[\sigma^2(F_o^2) + (P)^2]$ and $P = [F_o^2 + 2F_c^2]/3$.

Table 2 Selected bond lengths, contacts (Å) and angles (°) for **1**[a]

Ni1–O1	2.1229(19)
Ni1–O2	2.0349(18)
Ni1–O2b	2.0487(16)
Ni1–O2c	2.0972(18)
Ni1–N1	2.099(2)
Ni1–Cl1	2.3955(7)
Ni1 ··· Ni1a	3.0878(5)
Ni1 ··· Ni1b	3.1746(6)
Ni1 ··· Ni1c	3.0878(5)
Ni1–O2–Ni1a	98.25(7)
Ni1–O2c–Ni1a	96.27(7)
Ni1–O2–Ni1b	100.39(8)
Ni1–O2b–Ni1b	100.39(8)

[a] Symmetry transformations: a = 0.5+x, 0.5+y, 0.5+z. b = 1.25+y, 1.75–x, 0.75–z. c = 2.5–x, 1–y, 0.5+z.

of 100.4° (see Table 2). Each Ni_4 cubane is hydrogen-bonded to four neighbouring cubanes through two N–H ··· Cl contacts (N1–H5 ··· Cl1a = 3.33 Å) (see Fig. 2).

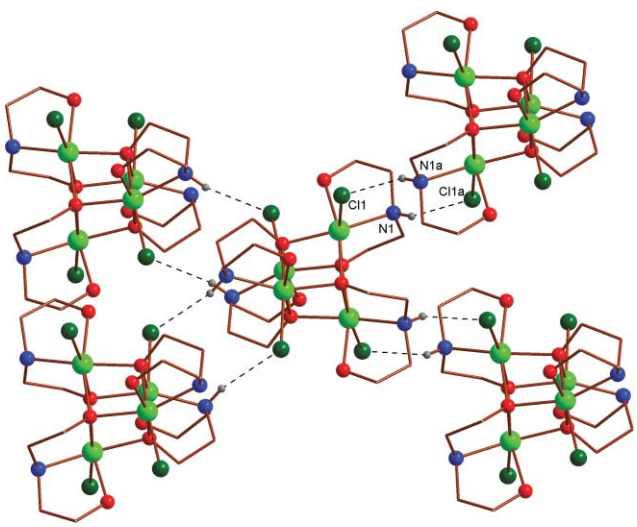

Fig. 2 Hydrogen bonding between neighbouring cubane clusters.

DC magnetic susceptibility measurements

DC magnetic susceptibility measurements were carried out on an air-dried sample, which analysed as **1**·3H_2O. A plot of χT *versus* temperature is shown in Fig. 3. The χT value at 300 K is 4.9 cm^3 mol^{-1} K and is consistent with four uncoupled Ni(II) ions with $g = 2.21$. χT increases gradually to a value of 6.9 cm^3 mol^{-1} K at 50K. Below 50K χT increases more sharply, reaching a maximum of 9.9 cm^3 mol^{-1} K at 11K, before dropping sharply to 3.8 cm^3 mol^{-1} K at 1.8K. The value of χT at 11K does not reach the expected value of 12.2 cm^3 mol^{-1} K for a spin ground state of $S = 4$ with $g = 2.21$. The value of χT at low temperature is affected by a large zero-field splitting (ZFS) and intermolecular interactions, which will be discussed in more depth in the following sections.

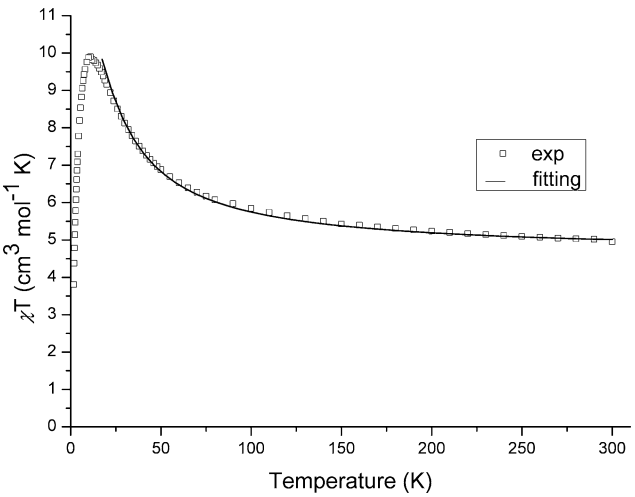

Fig. 3 Temperature dependence of χT from 300–1.8 K measured in a field of 1 kOe. The solid line represents a fit of the data in the range 300–17 K.

Consideration of the Ni–O–Ni bond angles within the cubane suggest that a minimum of two exchange interactions are required to model the magnetic behaviour of the complex. This conclusion was reached as magneto-structural correlations for Ni_4 cubanes show a change from ferromagnetic to antiferromagnetic exchange coupling at about 99°.[25] Therefore, we can describe the system using one J parameter for the interactions around the side faces (angles < 99 °), and another for the interactions on the top and bottom faces of the cubane (angles > 99°). This gives the spin Hamiltonian in eqn (1):

$$\hat{H} = -2J_1(\hat{S}_1\hat{S}_2 + \hat{S}_2\hat{S}_3 + \hat{S}_3\hat{S}_4 + \hat{S}_1\hat{S}_4) - 2J_2(\hat{S}_1\hat{S}_3 + \hat{S}_2\hat{S}_4) \quad (1)$$

The energies of the 19 spin states were calculated using Kambe methods and CAMMAG[26] used to fit the χT data above 17 K, to avoid ZFS and intermolecular interactions. The best fit gave a spin ground state of $S = 4$, with $g = 2.15$, $J1 = 7.29$ cm^{-1} and $J2 = -2.08$ cm^{-1}. $J1$ corresponds to the ferromagnetic exchange coupling on the four side faces of the cubane, as expected from magneto-structural correlations.

Magnetisation measurements

In order to estimate the ZFS parameter, D, magnetisation data were collected in the ranges 2–5 T and 2–7 K (Fig. 4). The data

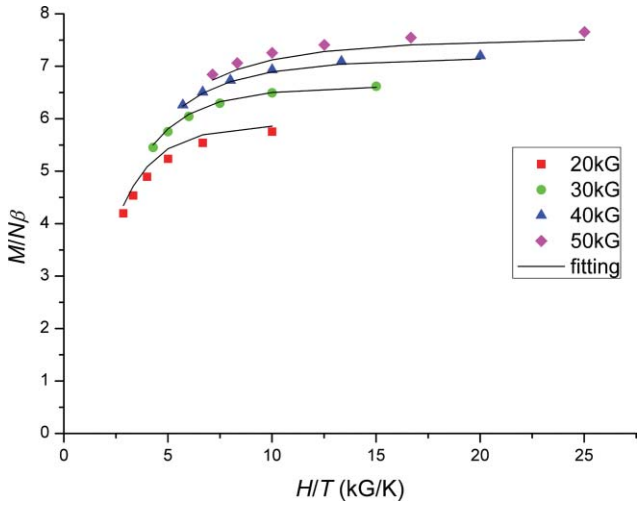

Fig. 4 Reduced magnetisation ($M/N\beta$) *vs* H/T in the field and temperature ranges 20–50 kG and 2–7 K. The solid lines correspond to a fit of the data with $S = 4$, $g = 2.07$ and $D = -0.70$ cm^{-1}.

were fit by a matrix diagonalization method using the program MAGMOFIT to a model that assumes only the ground state is populated, includes axial zero-field splitting ($D\hat{S}_z^2$) and the Zeeman interaction, and carries out a full powder average.[27] The corresponding Hamiltonian is given by eqn (2):

$$\hat{H} = D\hat{S}_z^2 + g\mu_B\mu_0\hat{S}H \quad (2)$$

Where D is the axial anisotropy, μ_B is the Bohr magneton, μ_0 is the vacuum permeability, $\hat{S}_z$ is the easy-axis spin operator, and H is the applied field. The best fit gave a spin ground state of $S = 4$ with $g = 2.07$ and $D = -0.70$ cm^{-1}. The negative sign of D indicates that there is an easy magnetisation axis and so we could expect the complex to display slow relaxation of magnetisation.

AC magnetic susceptibility measurements

AC magnetic susceptibility measurements were carried out to determine if **1** displays slow relaxation of magnetisation. Data was collected for frequencies in the range 130–9997 Hz in the temperature range 1.8–8 K. A frequency dependent out-of-phase signal is observed below 2.8 K (Fig. 5). The magnitude of the χ'' signal is around 20% of the χ' signal at 1.8 K and 9997 Hz.

Although no distinct peaks are observed the increase in the χ'' signal suggests that complex **1** shows slow relaxation of magnetisation.

Single-crystal high-frequency EPR spectroscopy

In order to confirm the spin ground state of the complex and determine the ZFS parameter, D, high-frequency EPR spectroscopy was carried out on a single crystal of **1**·4MeCN·4.5H_2O. The crystal was mounted in a rotating cavity where the plane of rotation was such that the magnetic field rotated from the *c*-axis of the crystal to the *ab* plane. To determine whether complex **1** showed the expected behaviour for a uniaxial system the temperature dependence was measured at 204.1 GHz with the field aligned approximately along the easy axis (Fig. 6).

The two plots shown in Fig. 6. confirm the spin ground state of $S = 4$ and that the axial ZFS parameter is negative. Fine structure

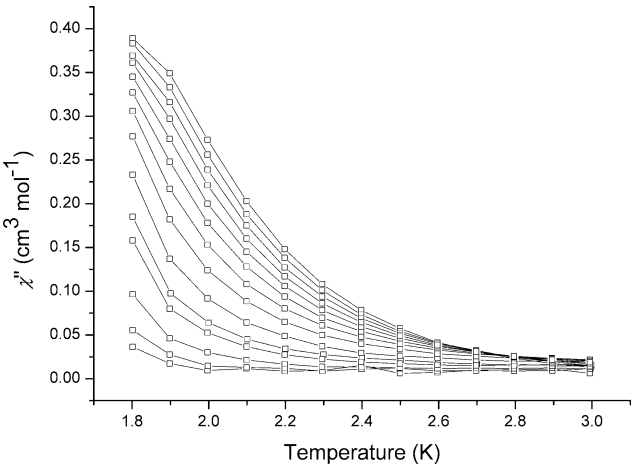

Fig. 5 Plot of χ'' *versus* T in the frequency range 130–9997 Hz.

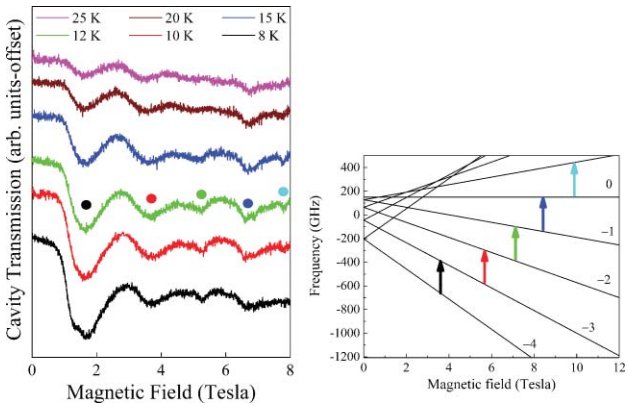

Fig. 6 The temperature dependence at 204.1 GHz with the field aligned along the easy-axis, where the coloured dots above the various resonances in the 12 K data correspond to the transitions shown in the Zeeman diagram for the magnetic field parallel to the *z*-axis.

transitions are seen that correspond to the $m_s = -4$ to $m_s = -3$, $m_s = -3$ to $m_s = -2$, *etc.* transitions. As the temperature is decreased the transitions at the lowest field become most intense and the peaks are evenly spaced, which indicates that D is negative. Measurement of the frequency dependence at 15 K with the field aligned along the easy-axis allowed an estimate of the *z*-component of the *g*-tensor by fitting each data set (see Fig. 7 left) with a linear regression and computing the *g*-value from the weighted average of the slopes. The value obtained was $g_z = 2.275$.

Using the obtained *g*-value the data was then re-fit to a simpler linear function [$f = \Delta_o(m) + g\mu_B B$] with just one adjustable parameter, $\Delta_o(m)$, the ZFS associated with each transition. This allowed the ZFS to be calculated for each transition and is plotted *versus* $(m + \frac{1}{2})$, where m is the state from which the transition was excited (Fig. 7 right). For a simple SMM, a polynomial fit to the ZFS plotted in this way should go through the origin ($\alpha = 0$), and only β and δ should be finite (see Fig. 7 right). However, this is not the case here suggesting additional physics could be present. Indeed, the finite-field intercept (finite α) found in Fig. 7 strongly suggests the presence of an internal exchange field (an exchange bias). Meanwhile, the values of β and δ obtained from the polynomial fit give: $D = -23.5$ GHz (-0.784 cm^{-1}) and $B_4^0 = -0.003$ GHz (-10^{-4} cm^{-1}). Initial attempts to fit the frequency

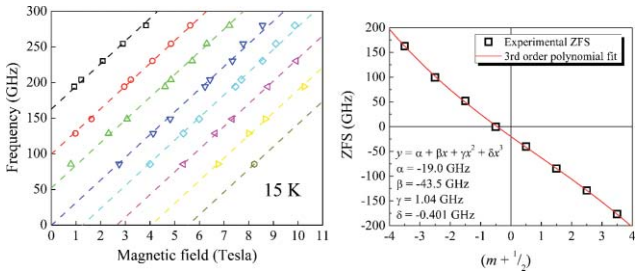

Fig. 7 Frequency dependence at 15 K with the field aligned along the easy-axis. Each data set is colour coded to indicate which transition is which (black = $m_s = -4$ to $m_s = -3$, through to gold = $m_s = 3$ to $m_s = 4$). Plot on right shows a cubic polynomial fit of the ZFS associated with each transition.

dependent data using the effective spin Hamiltonian (eqn (3)) were unsuccessful as this model did not include intermolecular exchange interactions.

$$\hat{H} = g_z\mu_B \cdot \hat{S}_z + D\hat{S}_z^2 + B_4^0\hat{O}_4^0 \quad (3)$$

To improve the model an antiferromagnetic exchange bias of 0.63 T was added to the fits obtained using the effective spin Hamiltonian (red dashed lines in Fig. 8).

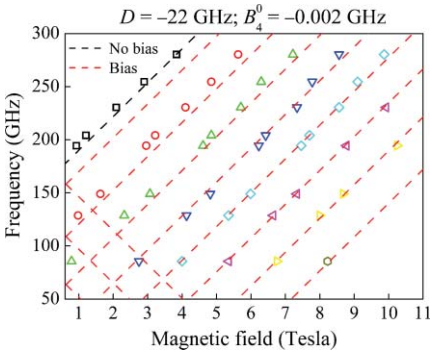

Fig. 8 Fit of the frequency dependent data using the effective spin Hamiltonian with an added antiferromagnetic exchange bias of 0.63 T.

This technique of adding an exchange bias to the model has been used before for a Mn_4 dimer that also displayed antiferromagnetic exchange interactions between molecules.[28] In this case it was found that mainly peaks observed at higher fields were affected by the exchange bias, which is comparable with the data for **1**; note that the modified fit is excellent for the highest field peaks, which are impossible to fit on the basis of eqn (3) alone. For Mn_4, the lowest field (ground state) transition was shown to occur at exactly the position where one would expect it based on the single-SMM model with no exchange bias (eqn (3)). This is also the case in our Ni_4 example as shown by the fit to the lowest transition using the model containing no exchange bias (black line in Fig. 8). The best fit parameters obtained were $D = -22.5 \pm 1.0$ GHz ≡ -0.75 ± 0.03 cm^{-1}, $B_4^0 = -0.002 \pm 0.001$ GHz ≡ $-(6.7 \pm 3.3) \times 10^{-5}$ cm^{-1}, and $g_z = 2.275$.

Low temperature magnetisation hysteresis

Magnetisation *versus* applied field hysteresis loops were obtained on single crystals of **1** using a micro-SQUID,[29] with the field oriented parallel to the easy axis of magnetisation of the crystal. Hysteresis loops are observed that are temperature dependent but only weakly sweep rate dependent (Fig. 9), confirming that **1** shows slow relaxation of magnetization. However, the S-shaped curve and the drop in sweep rate dependence from that observed for isolated SMMs is indicative of intermolecular interactions, which hinder quantum tunnelling at low temperature.[30] The Ni_4 crystals might also have lost solvent, which can cause a broadening of the hysteresis loops.

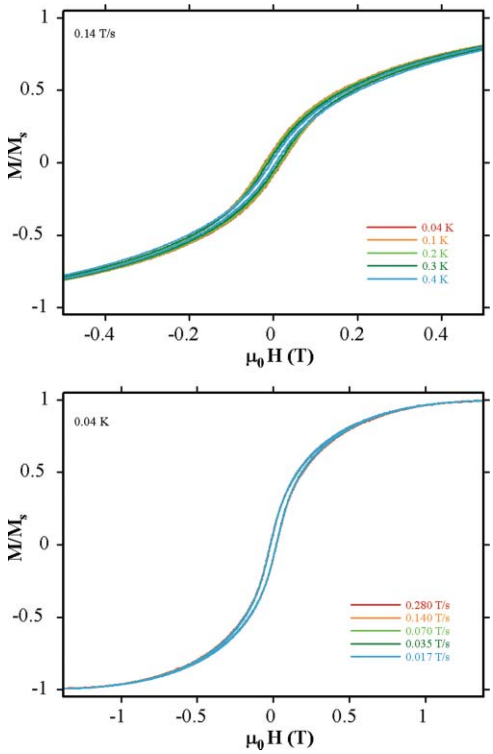

Fig. 9 Temperature dependent (top) and sweep rate dependent (bottom) hysteresis loops for single-crystals of **1**·4MeCN·4.5H_2O.

The presence of intermolecular interactions is consistent with the exchange bias between molecules observed in the high-frequency EPR measurements. The intermolecular interactions combined with a large ZFS also explain the slightly low value of χT at low temperature. As stated earlier, antiferromagnetic exchange bias is observed in a dimer of Mn_4 SMMs.[31] In this example the pairs of Mn_4 molecules are held together by six C–H···Cl (3.71 Å) hydrogen bonds and one Cl···Cl (3.858 Å) interaction. The Cl···Cl distances between neighbouring molecules of **1** is 4.663 Å and so this extremely weak interaction can probably be ignored. However, each cubane is involved in eight N–H···Cl (3.33 Å) hydrogen bonds between neighbouring molecules that are shorter than the C–H···Cl hydrogen bonds seen in the Mn_4 dimer. Although these hydrogen bonding interactions are weak individually when they are combined they will lead to a significant antiferromagnetic exchange interaction between neighbouring molecules, as is seen in the Mn_4 example. This is reflected in the larger exchange bias of 0.63 T seen for **1** compared to 0.33 T for the Mn_4 dimer. Efforts are underway to reduce the intermolecular interactions seen for **1** by adding bulky groups, such as phenyl rings to the DEA ligand. In addition, we will target the synthesis of the Zn_4 analogue to investigate the effects of doping/dilution.

This could help to isolate the individual clusters, reducing the exchange bias present and allowing the observation of steps in the magnetisation *versus* applied field hysteresis loops.

Conclusions

A new nickel(II) cubane has been described, with $S = 4$ and $D = -0.75$ cm^{-1}, which shows slow relaxation of the magnetisation. Hysteresis loops are observed in magnetisation *versus* applied field studies, however, these are complicated by intermolecular interactions between neighbouring molecules. A significant exchange bias between Ni_4 clusters of 0.63 T has been observed by single-crystal high-frequency EPR spectroscopy.

Acknowledgements

We thank the University of Glasgow and the EPSRC for financial support. Work at the University of Florida is supported by the US National Science Foundation (grant nos DMR0239481 and 0506946).

Notes and references

1 (*a*) R. Sessoli, H.-L. Tsai, A. R. Schake, S. Wang, J. B. Vincent, K. Folting, D. Gatteschi, G. Christou and D. N. Hendrickson, *J. Am. Chem. Soc.*, 1993, **115**, 1804; (*b*) R. Sessoli, D. Gatteschi, A. Caneschi and M. A. Novak, *Nature*, 1993, **365**, 141.
2 (*a*) S. Piligkos, G. Rajaraman, M. Soler, N. Kirchner, J. van Slageren, R. Bircher, S. Parsons, H-U. Güdel, J. Kortus, W. Wernsdorfer, G. Christou and E. K. Brechin, *J. Am. Chem. Soc.*, 2005, **127**, 5572; (*b*) N. Aliaga-Alcalde, R. S. Edwards, S. O. Hill, W. Wernsdorfer, K. Folting and G. Christou, *J. Am. Chem. Soc.*, 2004, **126**, 12503; (*c*) P. King, W. Wernsdorfer, K. A. Abboud and G. Christou, *Inorg. Chem.*, 2004, **43**, 7315; (*d*) A. J. Tasiopoulos, A. Vinslava, W. Wernsdorfer, K. A. Abboud and G. Christou, *Angew. Chem., Int. Ed.*, 2004, **43**, 2117; (*e*) T. C. Stamatatos, K. A. Abboud, W. Wernsdorfer and G. Christou, *Angew. Chem., Int. Ed.*, 2007, **46**, 884.
3 (*a*) M. Soler, W. Wernsdorfer, K. Folting, M. Pink and G. Christou, *J. Am. Chem. Soc.*, 2004, **126**, 2156; (*b*) M. Murugesu, M. Habrych, W. Wernsdorfer, K. A. Abboud and G. Christou, *J. Am. Chem. Soc.*, 2004, **126**, 4766; (*c*) L. M. Wittick, K. S. Murray, B. Moubaraki, S. R. Batten, L. Spiccia and K. J. Berry, *Dalton Trans.*, 2004, 1003.
4 C. Delfs, D. Gatteschi, L. Pardi, R. Sessoli, K. Wieghardt and D. Hanke, *Inorg. Chem.*, 1993, **32**, 3099.
5 (*a*) C. Cadiou, M. Murrie, C. Paulsen, V. Villar, W. Wernsdorfer and R. E. P. Winpenny, *Chem. Commun.*, 2001, 2666; (*b*) H. Andres, R. Basler, A. J. Blake, C. Cadiou, G. Chaboussant, C. M. Grant, H. U. Güdel, M. Murrie, S. Parsons, C. Paulsen, F. Semadini, V. Villar, W. Wernsdorfer and R. E. P. Winpenny, *Chem.–Eur. J.* , 2002, **8**, 4867; (*c*) S. T. Ochsenbein, M. Murrie, E. Rusanov, H. Stoeckli-Evans, C. Sekine and H. U. Güdel, *Inorg. Chem.*, 2002, **41**, 5133.
6 M. Murrie, S. J. Teat, H. Stoeckli-Evans and H. U. Güdel, *Angew. Chem., Int. Ed.*, 2003, **42**, 4653.
7 S. L. Castro, Z. Sun, C. M. Grant, J. C. Bollinger, D. N. Hendrickson and G. Christou, *J. Am. Chem. Soc.*, 1998, **120**, 2365.
8 C. J. Milios, A. Vinslava, W. Wernsdorfer, S. Moggach, S. Parsons, S. P. Perlepes, G. Christou and E. K. Brechin, *J. Am. Chem. Soc.*, 2007, **129**, 2754.
9 L. Bogani and W. Wernsdorfer, *Nat. Mater.*, 2008, **7**, 179.
10 (*a*) A. Ferguson, A. Parkin, J. Sanchez-Benitez, K. Kamenev, W. Wernsdorfer and M. Murrie, *Chem. Commun.*, 2007, **33**, 3473; (*b*) A. Ferguson, A. Parkin and M. Murrie, *Dalton Trans.*, 2006, 3627–3628; (*c*) A. Ferguson, J. McGregor, A. Parkin and M. Murrie, *Dalton Trans.*, 2008, 731.
11 (*a*) R. W. Saalfrank, I. Bernt, M. W. Chowdhry, F. Hampel and G. B. M. Vaughan, *Chem.–Eur. J.* , 2001, **7**, 2765; (*b*) R. W. Saalfrank, I. Bernt, E. Uller and F. Hampel, *Angew. Chem., Int. Ed. Engl.*, 1997, **36**, 2482; (*c*) R. W. Saalfrank, C. Deutscher, S. Sperner, T. Nakajima, A. M. Ako, E. Uller, F. Hampel and F. W. Heinemann, *Inorg. Chem.*, 2004, **43**, 4372.
12 (*a*) R. W. Saalfrank, I. Bernt and F. Hampel, *Chem.–Eur. J.* , 2001, **7**, 2770; (*b*) V. T. Yilmaz, A. Karadag, C. Thöne and R. Herbst-Irmer, *Acta. Crst.*, 2000, **C56**, 948.
13 D. Foguet-Albiol, K. A. Abboud and G. Christou, *Chem. Commun.*, 2005, 4282.
14 G. Aromí, S. Parsons, W. Wernsdorfer, E. K. Brechin and E. J. L. McInnes, *Chem. Commun.*, 2005, 5038.
15 A. Bell, G. Aromí, S. J. Teat, W. Wernsdorfer and R. E. P. Winpenny, *Chem. Commun.*, 2005, 2808.
16 H. Oshio, M. Nihei, S. Koizumi, T. Shiga, H. Nojiri, M. Nakano, N. Shirakawa and M. Akatsu, *J. Am. Chem. Soc.*, 2005, **127**, 4568.
17 (*a*) E-C. Yang, W. Wernsdorfer, S. Hill, R. S. Edwards, M. Nakano, S. Maccagnano, L. N. Zakharov, A. L. Rheingold, G. Christou and D. N. Hendrickson, *Polyhedron*, 2003, **22**, 1727; (*b*) E. del Barco, A. D. Kent, E-C. Yang and D. N. Hendrickson, *Polyhedron*, 2005, **24**, 2695; (*c*) D. N. Hendrickson, E-C. Yang, R. M. Isidro, C. Kirman, J. Lawrence, R. S. Edwards, S. Hill, A. Yamaguchi, H. Ishimoto, W. Wernsdorfer, C. Ramsey, N. Dalal and M. M. Olmstead, *Polyhedron*, 2005, **24**, 2280; (*d*) J. Lawrence, E-C. Yang, R. Edwards, M. M. Olmstead, C. Ramsey, N. S. Dalal, P. K. Gantzel, S. Hill and D. N. Hendrickson, *Inorg. Chem.*, 2008, **47**, 1965; (*e*) M. Moragues-Cánovas, M. Helliwell, L. Ricard, E. Rivière, W. Wernsdorfer, E. K. Brechin and T. Mallah, *Eur. J. Inorg. Chem.*, 2004, 2219.
18 W. Wernsdorfer, N. Aliaga-Alcalde, D. N. Hendrickson and G. Christou, *Nature*, 2002, **416**, 406.
19 A. Altomare, G. Cascarano, G. Giacovazzo, A. Guagliardi, M. C. Burla, G. Polidori and M. Camalli, *J. Appl. Crystallogr.*, 1994, **27**, 435.
20 P. W. Betteridge, J. R. Carruthers, R. I. Cooper, K. Prout and D. J. Watkin, *J. Appl. Crystallogr.*, 2003, **36**, 1487.
21 P. v.d. Sluis and A. L. Spek, *Acta Crystallogr*, 1990, **A46**, 194.
22 A. L. Spek, *PLATON*, A Multipurpose Crystallographic Tool, Utrecht University, Utrecht, The Netherlands, 1998.
23 W. Wernsdorfer, K. Hasselbach, A. Benoit, B. Barbara, D. Mailly, J. Tuaillon, J. P. Perez, V. Dupuis, J. P. Dupin, G. Guiraud and A. Perex, *J. Appl. Phys.*, 1995, **78**, 7192.
24 (*a*) M. Mola, S. Hill, P. Goy and M. Gross, *Rev. Sci. Instrum.*, 2000, **71**, 186; (*b*) S. Takahashi and S. Hill, *Rev. Sci. Instrum.*, 2005, **76**, 023114.
25 M. A. Halcrow, J-S. Sun, J. C. Huffman and G. Christou, *Inorg. Chem.*, 1995, **34**, 4167.
26 J. M. Rawson, *Cammag version 4.1*, University of Cambridge, 2005.
27 Dr S. Piligkos, University of Copenhagen.
28 S. Hill, R. S. Edwards, N. Aliaga-Alcalde and G. Christou, *Science*, 2002, **302**, 1015.
29 W. Wernsdorfer, *Adv. Chem. Phys.*, 2001, **118**, 99.
30 (*a*) M. Murugesu, R. Clérac, W. Wernsdorfer, C. E. Anson and A. K. Powell, *Angew. Chem., Int. Ed.*, 2005, **44**, 6678; (*b*) E. C. Yang, D. N. Hendrickson, W. Wernsdorfer, M. Nakano, L. N. Zakharov, R. D. Sommer, A. L. Rheingold, M. Ledezma-Gairaud and G. Christou, *J. Appl. Phys.*, 2002, **91**, 7382.
31 (*a*) A. Wilson, S. Hill, R. S. Edwards, N. Aliaga-Alcalde and G. Christou, *AIP Conf. Proc.*, 2006, **850**, 1141; (*b*) S. Hill and A. Wilson, *J. Low Temp. Phys.*, 2006, **142**, 267.

